JGR Oceans

RESEARCH ARTICLE
10.1029/2021JC017304

A Recirculating Eddy Promotes Subsurface Particle Retention in an Antarctic Biological Hotspot

K. Hudson[1], M. J. Oliver[1], J. Kohut[2], M. S. Dinniman[3], J. M. Klinck[3], C. Moffat[1], H. Statscewich[4], K. S. Bernard[5], and W. Fraser[6]

[1]College of Earth, Ocean, and Environment, University of Delaware, Lewes, DE, USA, [2]Department of Marine and Coastal Sciences, Rutgers, The State University of New Jersey, New Brunswick, NJ, USA, [3]Department of Ocean and Earth Sciences, Old Dominion University, Norfolk, VA, USA, [4]College of Fisheries and Ocean Sciences, University of Alaska, Fairbanks, Fairbanks, AK, USA, [5]College of Earth, Ocean, and Atmospheric Sciences, Oregon State University, Corvallis, OR, USA, [6]Polar Oceans Research Group, Sheridan, MT, USA

Key Points:

- Isopycnal doming over Palmer Deep Canyon suggests the presence of a closed, subsurface, cyclonic eddy over the canyon
- Subsurface eddy increases retention time of simulated particles at depth
- A persistent, subsurface particle layer, retained by the eddy, consists of individual detritus particles on the order of 70 microns

Supporting Information:

Supporting Information may be found in the online version of this article.

Correspondence to:

K. Hudson,
khudson@udel.edu

Citation:

Hudson, K., Oliver, M. J., Kohut, J., Dinniman, M. S., Klinck, J. M., Moffat, C., et al. (2021). A recirculating eddy promotes subsurface particle retention in an Antarctic biological hotspot. *Journal of Geophysical Research: Oceans*, *126*, e2021JC017304. https://doi.org/10.1029/2021JC017304

Received 23 FEB 2021
Accepted 16 OCT 2021

Abstract Palmer Deep Canyon is one of the biological hotspots associated with deep bathymetric features along the West Antarctic Peninsula. The upwelling of nutrient-rich Upper Circumpolar Deep Water to the surface mixed layer in the submarine canyon has been hypothesized to drive increased phytoplankton biomass, attracting krill, penguins and other top predators to the area. However, observations in Palmer Deep Canyon lack a clear *in-situ* upwelling signal, laboratory experiments do not illustrate a physiological response by phytoplankton to Upper Circumpolar Deep Water, and surface residence times are too short for phytoplankton populations to reasonably respond to any locally upwelled nutrients. This suggests that local upwelling may not be the mechanism that links Palmer Deep Canyon to increased biological activity. Previous observations of isopycnal doming within the canyon suggested that a subsurface recirculating feature may be present. Here, using *in-situ* measurements and a circulation model, we demonstrate that the presence of a recirculating eddy may contribute to the maintenance of the biological hotspot by increasing residence times at depth and retaining a distinct layer of biological particles. Neutrally buoyant particle simulations showed that residence times increase to ~175 days at 150 m within the canyon during the austral summer. *In-situ* particle scattering, flow cytometry, and water samples from within the subsurface eddy suggest that retained particles are detrital in nature. Our results suggest that this seasonal, retentive feature in Palmer Deep Canyon is important to the retention of biological material and may contribute to the maintenance of this hotspot.

Plain Language Summary Palmer Deep Canyon is an area of high biological activity along the West Antarctic Peninsula. These biological hotspots were once thought to be driven by the upwelling of deep, nutrient-rich water promoting phytoplankton growth. Previous observations illustrated a lack of upwelling within Palmer Deep Canyon and suggested that a subsurface feature may instead contribute to increased biological activity in the area. We found that a subsurface, closed eddy increases residence times of deep particles over Palmer Deep Canyon. This feature can retain particles through the productive summer months and may be important to the establishment of the biological hotspot.

1. Introduction

Palmer Deep Canyon (PDC) is the nearshore deep terminus of a cross-shelf canyon along the West Antarctic Peninsula (WAP; Figure 1). Like many similar canyons along the WAP, PDC is a known biological hotspot due to its association with high predator activity, particularly penguins (Carvalho et al., 2016, 2020; Fraser & Trivelpiece, 1996; Schofield et al., 2013). Some colonies of Adélie penguins in this region of the WAP have persisted on millennial timescales (Emslie & Patterson, 2007; Emslie et al., 1998), indicating that this location is a persistent focal point of upper trophic level activity. This led to the "canyon hypothesis" by Fraser and Trivelpiece (1996) that suggests that the physical oceanography in the area results from the presence of PDC and other canyons along the WAP and these unique processes drive the formation of the biological hotspots (Fraser & Trivelpiece, 1996; Schofield et al., 2013). Since the hypothesis was coined, polar researchers have searched for the driving mechanisms responsible for connecting canyons with increased biological activity.

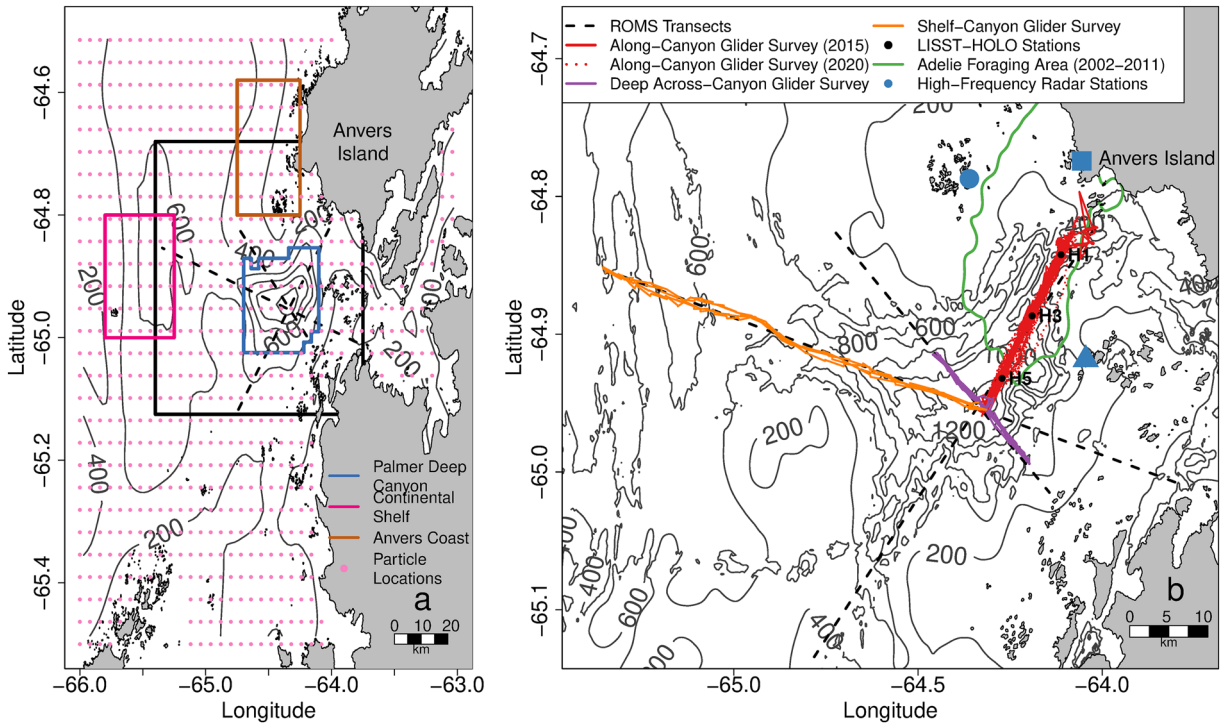

Figure 1. (a) Bathymetric map of Palmer Deep Canyon (PDC) and the surrounding shelf area. Bathymetry is Regional Ocean Modeling System (ROMS) bathymetry. Pink points illustrate where neutrally buoyant particles were seeded in ROMS experiments. The black box outlines the area shown in panel (b) The colored boxes indicate regions used for residence time calculations. (b) Bathymetric map of PDC and the glider transects from both field campaigns used in this analysis, with bathymetry from GMRT (Ryan et al., 2009). The black dashed lines in both panels indicate the corresponding transects used in ROMS. The green line represents the 99.5% contour for Adélie penguin foraging locations for penguins tagged between 2002 and 2011. The black circles indicate the locations of LISST-HOLO stations sampled in 2020. The blue shapes represent high-frequency radar locations at Palmer Station (square), Joubin Islands (circle), and Wauwerman Islands (triangle).

Prézelin et al. (2000, 2004) suggested that upwelling of deep, nutrient-rich Upper Circumpolar Deep Water (UCDW) on the continental shelf may promote phytoplankton blooms over the shelf, which could provide a sufficient food source for krill, a local keystone species and an important prey source for local penguin colonies. These upwelling regions, Prézelin et al. (2000) argued, were within the foraging range (100–150 km) for Adélie penguin populations based near PDC (Fraser & Trivelpiece, 1996). However, satellite telemetry of Adélie penguins nesting near PDC later revealed that these penguins forage within 20 km of their colonies, and specifically over PDC (Oliver et al., 2013, 2019; Pickett et al., 2018). This suggested that more localized physical processes may be responsible for the formation of the biological hotspot within PDC. With wind helping to move UCDW onto the shelf, cross-shelf canyons can act as conduits for UCDW transport onto the continental shelf (Dinniman et al., 2012; Martinson & McKee, 2012; Moffat et al., 2009). Autonomous gliders deployed within PDC observed shoaling of warm, subsurface waters over the canyon nearshore terminus (Schofield et al., 2013). They suggested this water mass was a modified derivative of UCDW (mUCDW), which can be transported onshore via subsurface eddies along canyons bisecting the continental shelf (Couto et al., 2017; Schofield et al., 2013). In addition, a multi-year analysis of satellite-derived sea ice concentration, sea surface temperature, and chlorophyll suggested that sea ice concentration was lower, sea surface temperature was higher, and chlorophyll was higher over PDC in comparison to nearby (~10 km) shelf areas (Kavanaugh et al., 2015). Together, these results suggested that mUCDW could be upwelling within the canyon, providing the warmth to melt surface sea ice and providing the nutrients to fuel phytoplankton blooms, which would in turn feed krill and their predators (Kavanaugh et al., 2015).

However, extended seasonal *in-situ* observations within PDC have suggested that local, seasonal upwelling of mUCDW may be rare in the canyon during the austral summer. Analysis of temperature and salinity properties from an extensive glider data set within PDC suggests that Winter Water (WW) acts as a barrier between the upward ventilation of mUCDW and the surface mixed layer in the austral summer (Carvalho

et al., 2016; Hudson et al., 2019). Carvalho et al. (2020) observed no significant changes in phytoplankton physiology when communities were exposed to nutrient-rich mUCDW indicating a light limited, rather than nutrient limited ecosystem. In addition, mUCDW is not a significant source of iron in this system (Sherrell et al., 2018). Furthermore, Kohut et al. (2018) calculated surface residence times within the penguin foraging grounds over PDC based on surface current measurements from a High-Frequency Radar (HFR) system and estimated surface residence times on the order of ∼2 days. Since the estimated local doubling time for phytoplankton is on the order of ∼7–70 days (Moline, 1998), they argued that observations of increased phytoplankton concentrations over the canyon could not be due to local episodic upwelling events because the surface residence time was too short for phytoplankton to grow in response to upwelled nutrients (Kohut et al., 2018).

Time series of the water mass properties suggest isopycnal doming is present, which led to the hypothesis that a subsurface recirculating eddy may be present within PDC (Hudson et al., 2019). Gliders deployed within PDC also observed a subsurface backscattering layer between 50 and 100 m where PDC was deeper than 500 m (Hudson et al., 2019). Hudson et al. (2019) hypothesized that this layer was made up of aggregations of marine snow, detrital particles greater than 500 μm (Alldredge & Silver, 1988), and other biogenic particles, possibly exported from the surface layer. This particle layer was observed throughout the glider deployments, suggesting that it could be retained within an eddy over PDC (Hudson et al., 2019).

Here, we test the hypotheses that a persistent subsurface eddy exists in PDC and is the likely explanation for the associated subsurface particle layer proposed by Hudson et al. (2019) using simulations of the WAP conducted with the Regional Ocean Modeling System (ROMS). We compare these simulations to glider deployments and surface measurements from a HFR system deployed in 2015 and 2020. First, we examine modeled and observed density properties and currents to show that a subsurface eddy exists within PDC. Second, we use particle simulations in ROMS to show that PDC has longer residence times compared to nearby regions due to the retentive subsurface eddy. Third, we use glider-measured optical backscatter and an Imaging Flow CytoBot (IFCB) to characterize the detrital particle layer that is retained within the canyon. If there is a subsurface eddy present within PDC, it could potentially act as a retaining feature for these detrital particles that could be a food resource for zooplankton.

2. Methods

2.1. Regional Ocean Modeling System

2.1.1. Model Simulations

ROMS (Haidvogel et al., 2008) was used to test the hypothesis that a subsurface eddy exists within PDC. The implementation of ROMS for the WAP (Graham et al., 2016) has 1.5 km horizontal resolution and 24 vertical layers. It includes a dynamic ice model (Budgell, 2005) and the interactions between floating ice shelves and the ocean (Dinniman et al., 2011; Holland & Jenkins, 1999). Atmospheric forcing is from archived forecasts from the Antarctic Mesoscale Prediction System (Powers et al., 2012). This model has two important updates from the version described in Graham et al. (2016). The base bathymetry (Bedmap2; Fretwell et al., 2013) was updated around Anvers Island (including PDC and the southern Gerlache Strait) using multibeam data (Ryan et al., 2009). Also, tidal forcing was added at the model lateral boundaries using tidal sea surface height and velocity from the CATS2008 regional Antarctic tidal model (Padman et al., 2002).

The model was run from November 2008 to April 2009. At the time of this analysis, ROMS simulations were not available for the two seasons of glider deployments (see Section 2.2). Since the model simulations were conducted for a different year than the glider observations, ROMS and glider data were averaged over the same seasonal time (early January to early March; see Section 2.2). The subsurface eddy is hypothesized to be a seasonal feature; therefore, we believe that this seasonal averaging will overcome the time misalignment between the model and *in-situ* data. Average temperature, salinity, and potential density (σ_θ) were calculated for each of the three transects (along-canyon, deep across-canyon, and shelf-canyon; Figure 1b). The averaged cross-sections were binned to the same horizontal resolution as the model (1.5 km). The vertical resolution was variable since ROMS depth layers are terrain following. These layers were translated to a 1 m vertical grid for plotting. Sea surface height (SSH) anomalies were calculated relative to the long-term model mean SSH. Current velocities and SSH were averaged in each model grid cell over the study region

(Figure 1b). Mixed Layer Depth (MLD) was estimated in each grid cell and averaged over PDC for each day using the maximum Brunt-Vaisala frequency (N^2; Carvalho et al., 2017).

2.1.2. Particle Simulations and Residence Time Calculations

Neutrally buoyant particles were released in the model simulation on a grid with approximately 4 km horizontal spacing around PDC (Figure 1a). The particles were advected by the model circulation at every model time step (50 s) using the full 3D velocity fields (at the time and position of each particle) plus a random walk in the vertical direction which is a function of the parameterized model vertical diffusion (Hunter et al., 1993; Visser, 1997). Particle positions were saved hourly. The vertical random walk was included for all particle releases, except for surface releases. Particles were released every 2 days starting on November 1, 2008 until the end of March 2009. All particle releases were tracked for a minimum of 30 days and a total of 64,800 particles were released. Particles were released at the surface, 10, 20, 50, 120, 150, and 300 m.

Residence times were calculated using e-folding time which is the time needed for the concentration of particles to drop to 1/e (~37%) within a defined region (Couto et al., 2017; Kohut et al., 2018; Piñones et al., 2011). Residence times were calculated in three regions: PDC, the continental shelf, and the coast of Anvers Island (Figure 1a). The 400 m isobath from ROMS was used to define PDC. The residence time was calculated for each particle release event from December 2008 to February 2009 to focus on the austral summer when predator foraging activity within PDC is highest (Smith et al., 1995). Residence times were compared in R with a Kruskal-Wallis test and Dunn post-hoc test with Bonferroni correction for multiple tests (R Core Team, 2020).

2.2. Glider Data Collection

The glider data used in this analysis were collected in the 2015 and 2020 austral summers (Table S1 in Supporting Information S1). The 2015 glider deployments and data are described in Hudson et al. (2019) and are re-presented here for comparison with the 2020 data (Table S1 in Supporting Information S1). We utilize the 2015 glider data collected on the along-canyon transect from January 11 to February 8, 2015 with a total of 1,415 profiles. Only temperature, salinity, σ_θ, chlorophyll, and optical backscatter variables are presented from the 2015 glider data set.

In the austral summer of 2020, three Slocum gliders were deployed. Two of the three gliders were deployed on January 9 2020 and the third glider was deployed on January 11, 2020. One of the gliders was recovered on February 26 and the remaining two gliders were recovered by March 11, 2020. For this analysis, we focus on the following transects covered by the three gliders during this time period: the along-canyon transect, from the head of the canyon to the deepest portion of the canyon; the deep across-canyon transect, which ran perpendicular to the along-canyon transect over the deepest portion of PDC; and the shelf-canyon transect, which traveled from the deepest portion of the canyon, over the canyon sill, to the continental shelf (Figure 1b). The same along-canyon transect was sampled in 2015 and 2020. The deep across-canyon and shelf-canyon lines were sampled opportunistically in 2020. The deep across-canyon transect was sampled a total of four times between January 14 and March 3 2020. The shelf-canyon transect was sampled twice between January 22 and February 11, 2020. In 2020, a total of 1,214 profiles were completed on the along-canyon transect. On the deep across-canyon transect, 139 profiles were completed, and 197 profiles were completed on the shelf-canyon transect. In 2015, the along-canyon transect was sampled to 200 m, while in 2020, this transect was sampled to 1,000 m. Both the shelf-canyon and deep across-canyon transect were sampled to 1,000 m. Deployment statistics for these transects in both study years are summarized in Table S1 in Supporting Information S1.

Each glider was equipped with a pumped SeaBird conductivity, temperature, and depth (CTD) sensor and a WetLabs Ecopuck, which measured optical backscatter at 700 nm and chlorophyll concentration. Gliders also measured oxygen saturation with an Aanderaa or RinkoII optode. The SeaBird CTDs were factory calibrated in August 2014, January 2019, and April 2019. Optical data from the gliders were cross-calibrated when the gliders were in close proximity with each other (Text S1, Equations S1–S4, Figure S1 in Supporting Information S1), similar to Hudson et al. (2019). Temperature and salinity properties were used to calculate σ_θ, with the *swSigma0* function in R package *oce* (Kelley & Richards, 2020; R Core Team, 2020). Optical data

were only collected on upcasts. Glider data from both field seasons was geolocated with bathymetry data from Ryan et al. (2009).

Average cross sections were generated by averaging *in-situ* measurements in 1.5 km horizontal bins and 1 m vertical bins. This was done separately for each year. Stratification strength was estimated using N^2, calculated using the *swN2* function in *oce* (Kelley & Richards, 2020; R Core Team, 2020). The max N^2 was used to estimate MLD and was calculated for each individual glider profile on the along-canyon transects in 2015 and 2020 (Carvalho et al., 2017). Only profiles deeper than 50 m were considered following Carvalho et al. (2017).

2.3. High-Frequency Radar

A HFR system was deployed around PDC in 2015 and 2020 (Figure 1b). The 2015 deployment is described in Kohut et al. (2018) and the 2020 deployment of this system was the same for the purposes of data collection. This system measures surface currents by analyzing and processing Bragg peaks of backscattered radio waves (Barrick et al., 1985; Kohut et al., 2018). The HFR located at Palmer Station operated at 13 MHz to allow the HFR to see past the nearshore islands between Palmer Station and PDC. The remaining two HFR stations operated at 25 MHz. The system produced hourly current maps on a 1×1 km resolution over PDC and had an effective depth of 0.5 m (Kohut et al., 2018). These currents are believed to be representative of currents within the mixed layer in PDC and the surrounding region (Carvalho et al., 2017; Kohut et al., 2018). The 2015 data were used previously to calculate surface residence times in Kohut et al. (2018), however the current velocity fields have not yet been examined. We present them here to compare observed velocity fields to those from ROMS.

Weather stations were deployed with the HFR stations to measure wind speeds. Using this wind data, we averaged the HFR field in periods when winds were low (< 5 m s^{-1}) at the Joubin and Wauwerman Islands (Figure 1b) for at least 12 hrs. We chose to average over low wind periods to avoid the influence of wind on surface currents (Kohut et al., 2018). Winds are also highly variable in this system and can vary significantly between the Joubin and Wauwerman sides of the canyon (Hudson et al., 2019; Kohut et al., 2018), so we averaged HFR data when winds were low on both sides of the canyon. Winds are likely stronger and more variable than ROMS captures, so we chose to make this comparison when external wind forcing is low. We believe that this will also help with the temporal mismatch between model and observation years.

2.4. Imaging Flow CytoBot

An IFCB was utilized to characterize the subsurface particle layer. The first sampling event occurred on February 8, 2020, and the second occurred on March 7, 2020. For both sampling events, stations HOLO 5, 3, and 1 were sampled (Figure 1b). A Rosette equipped with a SeaBird SBE-19 Plus V2 CTD (factory calibrated July 2019) and 6 Niskin bottles was deployed to 200 m. Bottles fired at 5, 35, 75, 100, 150, and 200 m on the upcast for both sampling events. Water from each depth was collected in dark 50 ml Falcon tubes. The Falcon tubes were triple rinsed with sample water before samples were collected and samples were kept dark and cold until processed.

Images were collected with the scattering (PMTA) and chlorophyll (PMTB) sensors. Sensitivities were increased to maximize photo collection without producing high numbers of photos with no targets, following the Palmer Long Term Ecological Research (LTER) program protocol. Blob and feature extraction were performed using the MATLAB IFCB Toolbox (Olson & Sosik, 2007; https://github.com/hsosik/ifcb-analysis/wiki). Data were matched to CTD profiles.

To estimate numbers of live versus detrital cells, we used PMTB to classify cells. Any images with PMTB greater than 0.01 (~77% quantile) were classified as live cells. This threshold was based on the distribution of PMTB values and glider-observed chlorophyll concentrations. Equivalent diameter, estimated by the IFCB Toolbox, was used to estimate particle size.

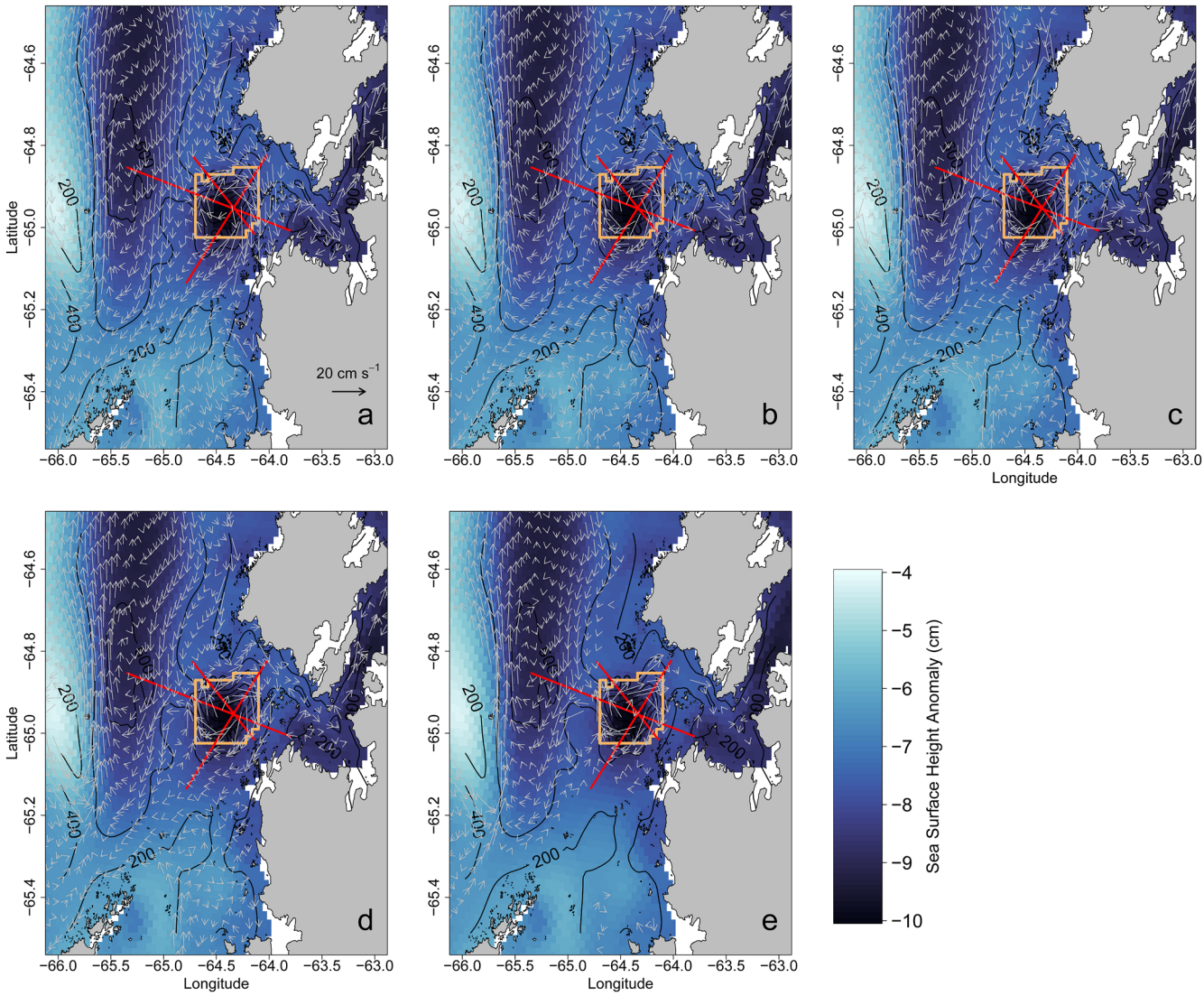

Figure 2. Average current velocity at surface (a), 50 (b), 100 (c), 150 (d), and 300 m (e) in cm s-1 over Regional Ocean Modeling System (ROMS) model domain used in this study from January to March 2009. Color indicates the mean sea surface height anomaly (cm) from ROMS over the same time period. Red lines indicate the location of ROMS average transects. Every eighth model vector is plotted. The orange box illustrates the region used to calculate residence time over Palmer Deep Canyon (PDC) as in Figure 1a.

3. Results

3.1. Subsurface Eddy

3.1.1. ROMS Simulations

Average velocity vectors over PDC in the austral summer show a relatively strong (~10 cm s^{-1}), cyclonic circulation over the canyon (Figure 2 and Movie S1). This circulation pattern is present across several depths (0, 50, 100, 150, and 300 m; Figure 2). At shallower depths (0 and 50 m), the mean cyclonic circulation stretches south of the canyon (Figures 2a and 2b). Daily averages show a great deal of variability, especially close to the surface, and many periods where there is not closed circulation over the canyon (Movie S1). As depth increases, the circulation associated with the eddy becomes more aligned with isobaths and its horizontal extent more limited with respect to surface flow (Figures 2c–2e). In this particular year (2008–2009), the eddy forms in late December and is no longer a coherent feature after late February (Movie S1). The rotation appears at a similar time the following summer (not shown), which is consistent with the flow of the

eddy being approximately in geostrophic balance. Mean SSH over the same period is depressed by ∼−9 cm over PDC and mean flow at all depths was cyclonic around this low-pressure system (Figure 2).

Isopycnals from ROMS on the along-canyon (Figure 3a) and shelf-canyon (Figure 3b) transects begin to rise over the canyon between approximately 100 and 200 m. In both transects, the isopycnals gradually shallow on the southern and western flanks of the canyon, respectively (Figures 3a and 3b). Over the sill separating the canyon from the continental shelf, isopycnals are spaced more evenly in the top 400 m than over PDC, possibly indicative of isopycnal stretching (Figure 3b). On the deep-across canyon transect, the model suggests a slight depression of isopycnals beginning just above 100 m, approximately 23 km into the transect (Figure 3c). There is also a slight lift in isopycnals on the west flank of the canyon, approximately 15 km along the transect, however, the isopyncals were relatively flat over this transect (Figure 3c). Average temperature transects illustrate a WW layer over the deeper portions of the canyon (Figure S2 in Supporting Information S1) and on the shelf (Figure S2 in Supporting Information S1). Isothermals lift along the edges of the canyon (Figure S2 in Supporting Information S1). Isohaline patterns follow changes in density over all transects (Figure S3 in Supporting Information S1).

3.1.2. Glider Observations

Gliders in both field campaigns observed similar density structures as the modeled fields (Figures 3 and 4, S4 in Supporting Information S1). Above 100 m, ROMS waters were between ∼27.3 and 27.5 σ_θ across all three transects while gliders observed waters ranging between ∼27.1 and 27.5 σ_θ across all transects and field campaigns (Figures 3 and 4). Waters from 100 to 400 m in ROMS ranged from 27.5 to ∼27.75 σ_θ while gliders observed deep waters between 27.5 and over 27.9 σ_θ (Figures 3 and 4). Overall, waters were ∼0.2 σ_θ lighter in the surface and ∼0.15 σ_θ heavier between 100 and 400 m in the *in-situ* observations in comparison to ROMS (Figures 3 and 4). These density differences in surface waters and waters below the mixed layer, specifically the mUCDW, are likely due to differences in the salinity (Figures 4a–4b; S2, S3, S5a–S5b and S6a-S6b in Supporting Information S1).

In 2015, stratification decreased on the along-canyon transect over the course of the glider deployment (Figure S7a in Supporting Information S1) while stratification strengthened slightly over time in 2020 (Figures S4 and S7b in Supporting Information S1). Stratification was weaker in early January 2020 likely because of stronger winds early in the season and a warmer, fresher WW layer (Figures S7b, S8 and S9 in Supporting Information S1). On average, the surface mixed layer was fresher, warmer, and deeper in 2020 (Figures S5–S6 and S8–S9 in Supporting Information S1), resulting in some isopycnals being deeper than in 2015 (Figure 4). Since the mixed layer was deeper in 2020, the WW layer was also deeper, which likely played a role in the different isopycnal depths (Figures 4 and S8 in Supporting Information S1).

The along-canyon transects observed similar uplift of isopycnals over the deepest portions of the canyon in both years (Figures 4a and 4b). Isopycnals slowly rose near the edge of the canyon (∼10 km into the transect; Figures 4a and 4b). This uplilft was most pronounced between 50 and 100 m in 2015 and 50 and 150 m in 2020 (Figures 4a and 4b). The uplift was present, but more gradual below these depths (Figures 4a and 4b).

The uplift of isopycnals over the canyon was also observed on the shelf-canyon line (Figure 4c). This uplift was most prominent in the top 150 m (Figures 4b and 4c). The isopycnals also stretch as they move from the continental shelf into the canyon and this is more pronounced in ROMS (Figures 3b and 4c). On the deep across-canyon line, the isopycnals gradually deepen on the western flank of the canyon (Figure 4d). There is no small dip in isopycnal depth mid-canyon in the glider observations like in model simulations (Figures 3c and 4d; S2c and S5d in Supporting Information S1).

Oxygen saturation reached a minimum of 50% over the deeper portions of the canyon in 2020 (Figure S10 in Supporting Information S1). Low oxygen saturation (< 70%) was generally observed higher in the water column over these areas, especially on the along-canyon and shelf-canyon transects (Figure S10a–S10b in Supporting Information S1).

3.1.3. High-Frequency Radar Observations

To examine the surface expression of the eddy over the canyon, we examined the HFR data sampled in low wind periods to limit the effect of winds on the observed currents. There were 7 periods in 2015 and 10

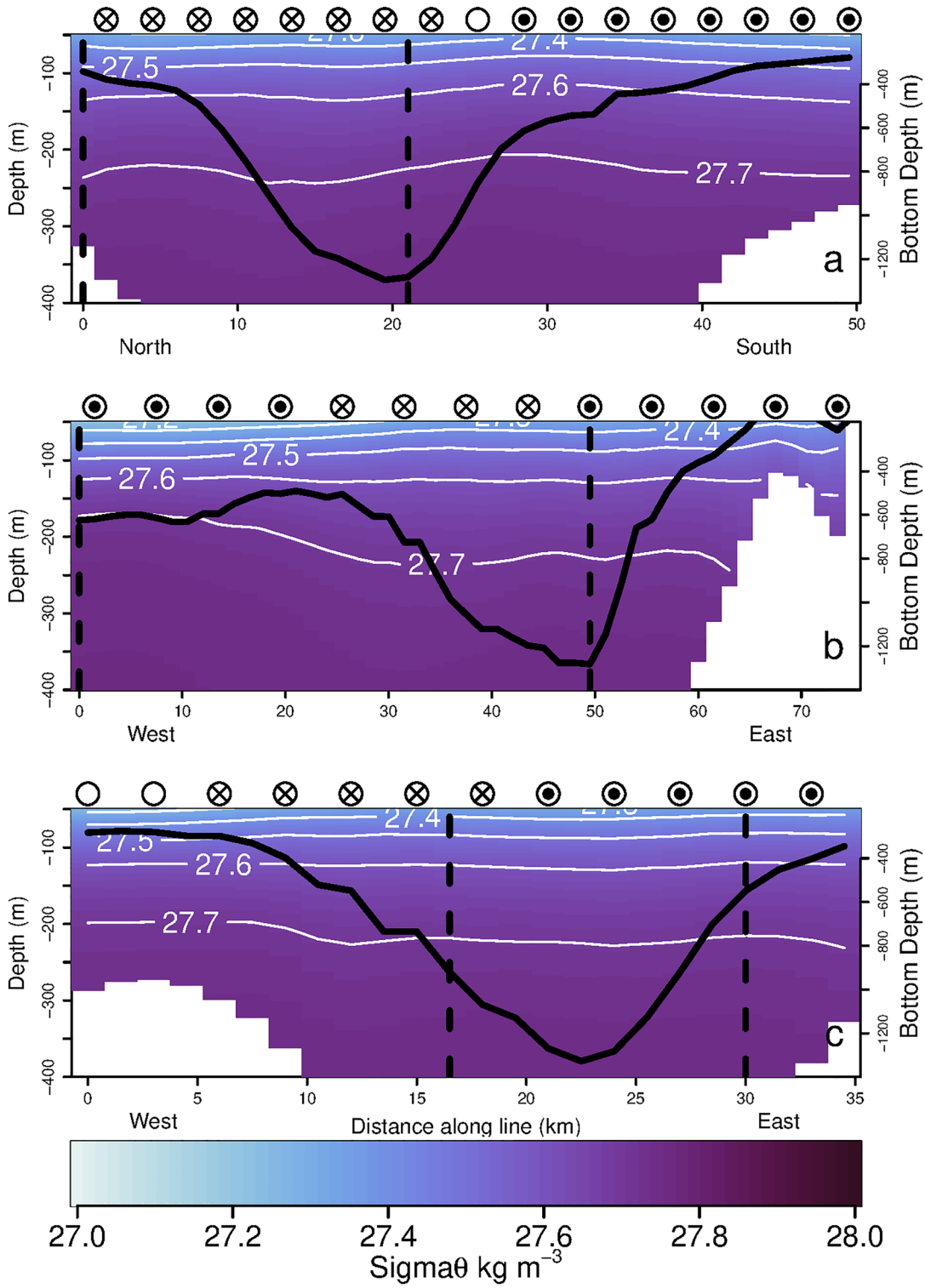

Figure 3. Average σ_θ cross sections with 0.1 σ_θ contour lines from the along-canyon (a), shelf-canyon (b), and deep across-canyon (c) transects in Regional Ocean Modeling System (ROMS) simulation. The start of the transects (0 km) indicates the northern (a) and western (b and c) sides of the transects. Observations were averaged in 1.5 km bins in the horizontal. In the vertical, data were averaged over the model's 24 vertical depth bins and translated to 1 m depth bins for plotting. Points above each plot indicate general flow into (circles containing an "x") or out of (circles containing a point) the cross section as illustrated in Figure 2. Empty circles indicate flow parallel to the transect. The black line denotes the model bathymetry and corresponds to the right *y* axis in each panel. Note that each panel starts at 50m. Vertical dashed black lines indicate the regions of the transects that were occupied by the gliders.

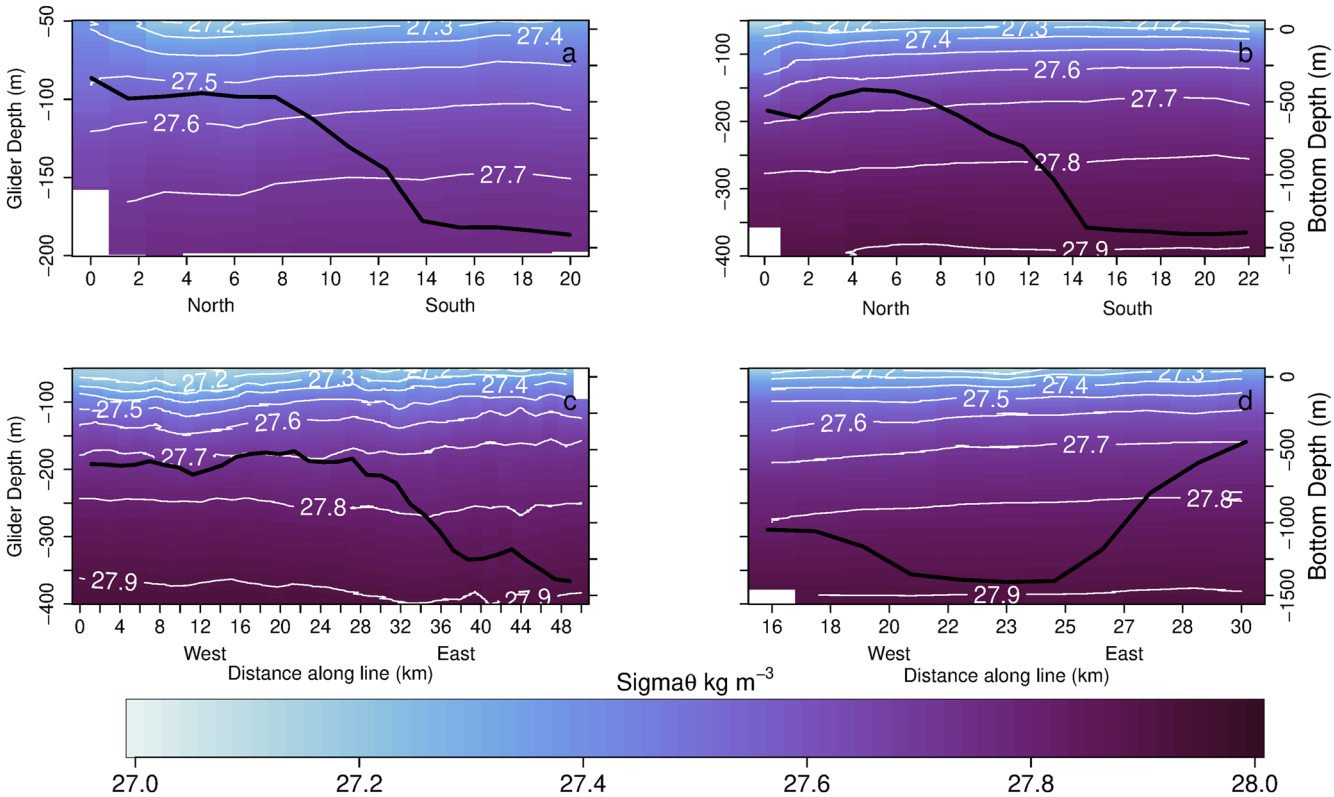

Figure 4. Average σ_θ cross sections with 0.1 σ_θ contour lines from the along-canyon (a and b), shelf-canyon (c), and deep across-canyon (d) transects observed by gliders in 2015 (a) and 2020 (b–d). Distances along lines correspond to the distances along Regional Ocean Modeling System (ROMS) transects in Figure 3. Observations were averaged in 1.5 km bins in the horizontal and 1 m bins in the vertical. The black line denotes the average canyon depth experienced by the glider and corresponds to the right *y* axis in each panel. Note that each panel starts at 50 m and that transects from 2015 (a) are only plotted to 200 m while the remaining panels are plotted to 400 m.

periods in 2020 of low winds (< 5 m s^{-1}) over the canyon (Figure S7 in Supporting Information S1). These time periods ranged from 12 to 100 h long (Figure S7 in Supporting Information S1). Across both years, most of these periods were dominated by strong surface currents from the southeast moving toward the northwest.

Two periods, one in each year, showed cyclonic rotation over the canyon (Figure 5; regions shaded with dark gray lines in Figure S7 in Supporting Information S1). In 2015, this period occurred in late January and was 22 h in length (Figure 5a and S7a). In 2020, cyclonic rotation was observed in early January (Figure S7b in Supporting Information S1) and was the longest low wind period (100 h) considered (Figure 5b and S7b in Supporting Information S1). These low-wind incidences co-occurred with periods of weak stratification (Figure S7 in Supporting Information S1).

In comparison to ROMS (Figure 2a), HFR measured current velocities were more similar in 2015 than in 2020. ROMS surface currents over PDC and the coast of Anvers Island were close to 20 cm s^{-1} on average, while HFR measured surface currents ranged between 10 and 20 cm s^{-1} in the same area in 2015 (Figure 5a). High (~20 cm s^{-1}) currents were located along the coast of Anvers Island in both the model and observed current velocity fields. In 2020, surface currents measured by the HFR were ~5–10 cm s^{-1} throughout the HFR domain, approximately half of the velocities estimated by ROMS in the same region (Figures 2a and 5b).

3.2. Residence Times Over PDC

Residence times over PDC generally increased with depth (Figure 6). Median residence times (±1 standard deviation) increased from 4.1 ± 3.3 days at the surface to 166.6 ± 74 days at 150 m (Figure 6). Residence

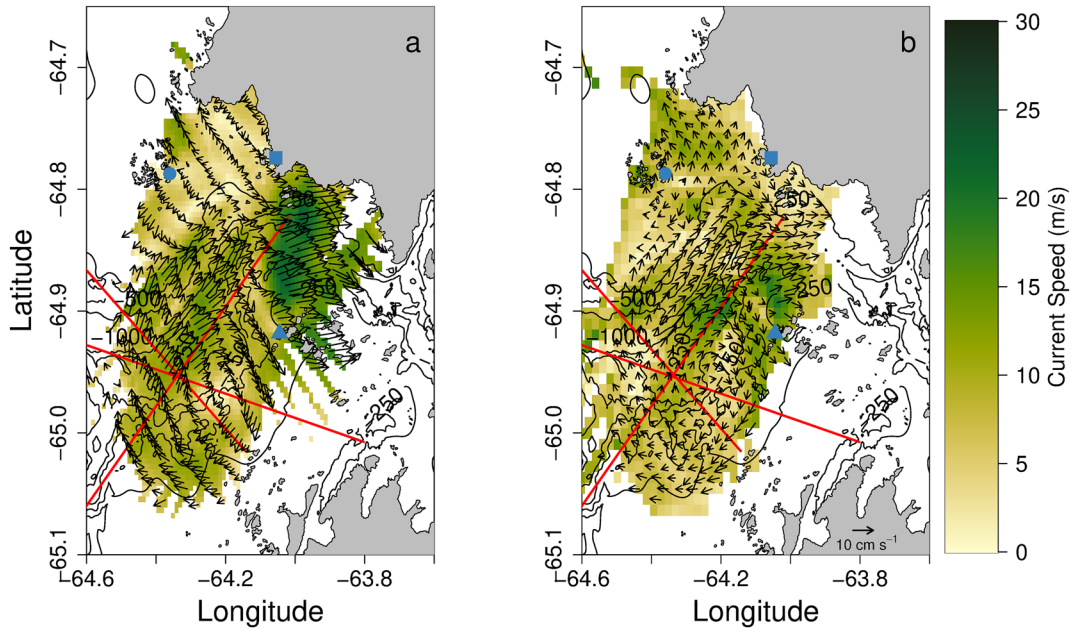

Figure 5. Mean High-Frequency Radar (HFR) fields over Palmer Deep Canyon during two low-wind periods in 2015 (a) and 2020 (b). Every 8th (a) and 2nd (b) vectors are plotted (the difference is due to data being gridded differently between 2015 and 2020). HFR stations are marked with blue shapes and are the same as in Figure 1b. The red lines are the Regional Ocean Modeling System (ROMS) transects from Figure 1.

times were 132.3 ± 26.1 days at 300 m but were not statistically different from the residence times at 150 m (Figure 6). Median residence times increase dramatically below 50 m, increasing from 18 ± 10.2 days at 50 m to 157.2 ± 86.8 days at 120 m. These residence times were much higher than those calculated on

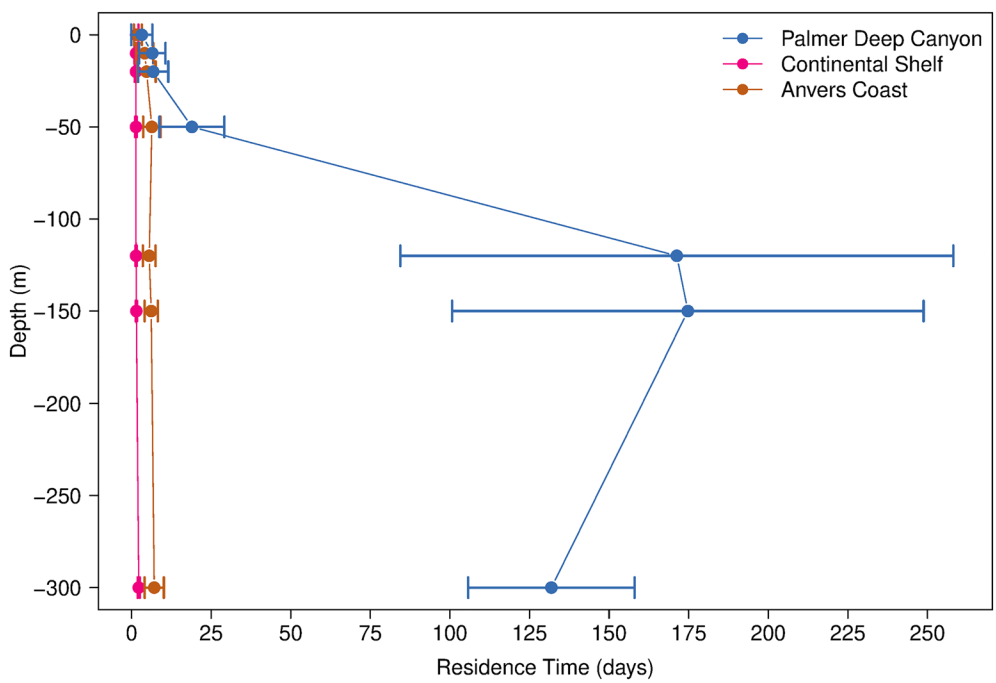

Figure 6. Median residence times (±1 Standard Deviation) of summertime simulated particles released in Regional Ocean Modeling System (ROMS) at the surface, 10, 20, 50, 120, 150, and 300 m during the 2008–2009 season within the Palmer Deep Canyon (blue), continental shelf (pink), and Anvers Coast (gold) regions defined in Figure 1a.

the continental shelf and the coast of Anvers Island (Figure 6). Residence times on the continental shelf ranged between 1.5 ± 0.7 and 2.3 ± 0.3 days over the same depths while they ranged between 2 ± 1.2 and 7.1 ± 3 days on the coast of Anvers Island (Figure 6). Residence times in the top 20 m over PDC and the Anvers coast were similar, but differed below 50 m (Figure 6).

The residence times over PDC differed significantly with depth ($p << 0.001$). In the top 50 m, residence times were not significantly different from each other ($0.107 < p < 1$). The only exception was that the surface and 50 m residence times differed significantly ($p < 0.001$). Similarly, residence times calculated between 120 and 150 m did not differ significantly ($p = 1$). However, when residence times were compared across shallow (≤ 50 m) and deep (≥ 50 m) particle releases, all comparisons differed significantly ($p << 0.001$). In comparison, only residence times on the continental shelf at 300 m were significantly different from other depths ($p << 0.001$). On the coast of Anvers Island, surface residence times were significantly lower than all other depths ($p << 0.001$). Residence times at 10 m were also significantly different from those at 300 m in this region ($p = 0.002$).

From December to February, shallow residence times (surface, 10, and 20 m) are similar, increasing to a maximum of approximately 20 days in January (Figure S11 in Supporting Information S1). Residence times at 50 m are similar to residence times at shallower depths until late December, where the residence times increase to ∼25–30 days until the end of the summer (Figure S11 in Supporting Information S1). At 120 and 150 m, residence times increase from 10-20 days in early December to upwards of 300 days in mid-December and decrease to 100–200 days at the end of the austral summer (Figure S11 in Supporting Information S1). The ROMS MLD shoals in late December when residence times at depth increase rapidly (Figure S12 in Supporting Information S1). At 300 m, residence times are constant throughout the austral summer, ranging between ∼100 and 175 days, with no correlation to stratification (Figure S11 in Supporting Information S1).

3.3. Subsurface Particle Layer

3.3.1. Glider Observations

The gliders observed a subsurface particle layer at ∼75–120 m in 2015 and 2020 (Figure 7). Optical backscatter was higher in 2015 in comparison to 2020 (Figure S13 in Supporting Information S1), possibly due to higher chlorophyll and particles in the mixed layer in 2015 (Figures S13 and S15 in Supporting Information S1). Regardless, the spatial patterns are similar between the along-canyon transects sampled in both years (Figures 7a and 7b). Increased optical backscatter (likely more particles) was observed over the deeper portions of the along-canyon transects (Figures 7a and 7b). On the shelf-canyon line (Figure 7c), increased particle concentrations were observed over the sill separating the canyon from the continental shelf. There was lower optical backscatter on the continental shelf in comparison to in the canyon (Figure 7c), suggesting that the eddy in PDC is retaining these particles. On this transect, particle concentrations at depth were significantly higher in PDC than on the shelf (Wilcoxon Rank Sum test, $p << 0.001$). Higher particle concentrations were also observed on the deep across-canyon transect over the deeper portions of the canyon at similar depths to the layer observed in the along-canyon transect (Figures 7b and 7d).

3.3.2. Identifying the Particles

In early February (Figures 8a–8c), live cell counts were highest in the surface and decreased with depth. At all stations and depths, detritus cells outnumbered live cells (Figures 8a–8c). At all three stations sampled, detritus cells increased below 100 m (Figures 8a–8c). This increase was most prevalent at H3 and H5 (Figures 8b and 8c). On March 6 (Figures 8d–8f), there were more live cells in the surface layer at all stations. This coincides with an increase in surface biomass (Figures S13–S14 and S16 in Supporting Information S1). Particle counts of live cells still decreased with depth (Figures 8a–8c). There were more detritus cells throughout the water column in the second sampling event in comparison to the first sampling event (Figure 8). At H5 and H3, the number of detrital cells increased dramatically at 75 m in comparison to H1 (Figures 8d–8f). This was shallower than the previous sampling event, where detritus particles started to increase at 100 m at these stations (Figures 8b and 8c), suggesting that the particle layer had shallowed over the canyon between sampling events.

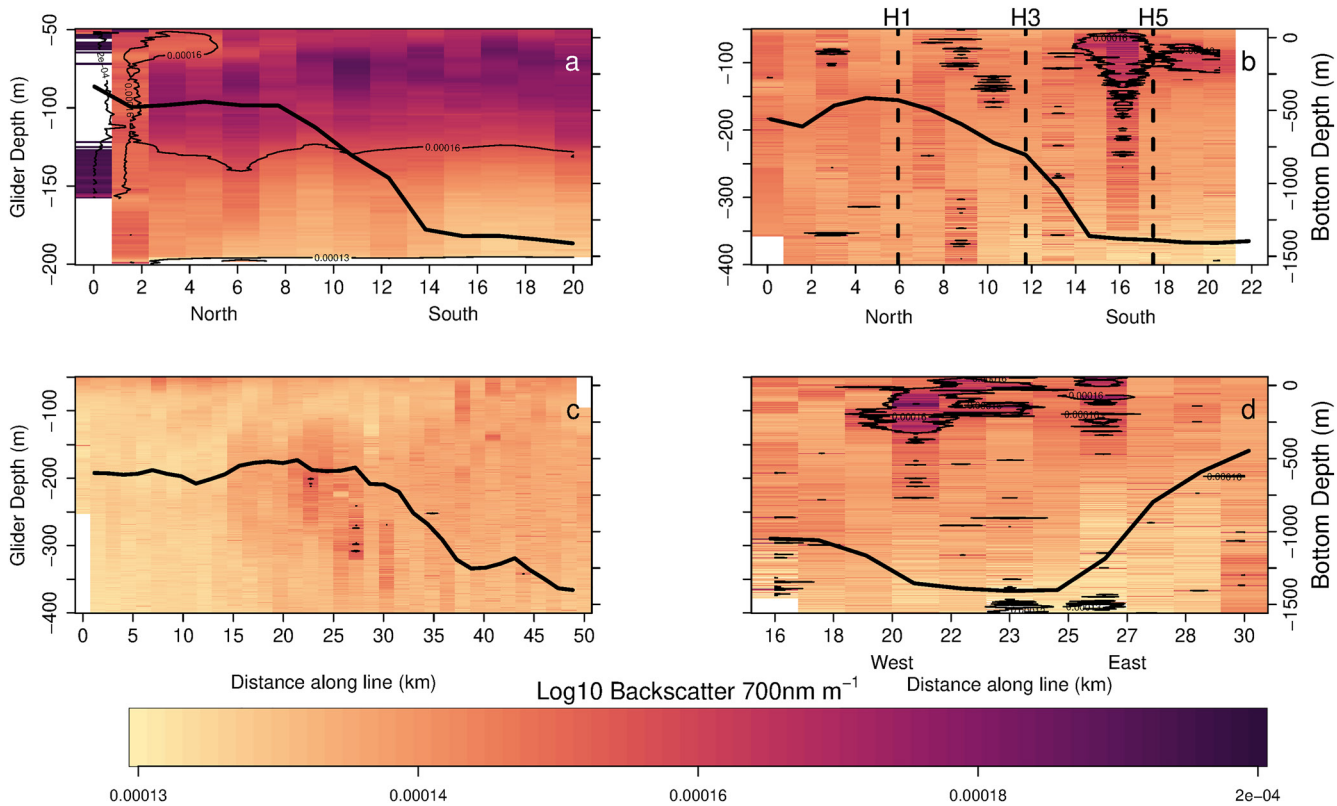

Figure 7. As in Figure 4, but with optical backscatter and 0.1 contours (in log10 space). Vertical lines in panel b indicate the locations of the HOLO stations sampled in 2020.

Particles between 75 and 200 m (Figures 7 and 8) were predominately detrital, with live cells comprising a small percent of all cells within the layer across both sampling events (Figure 8). Images from the IFCB confirm that these particles are detritus with many being amorphous (Figure 8, insets). Some particles look like small conglomerates (Figure 8b, detritus example from 200 m), while others look like clear material that may have been sloughed off in a molting event, or remains of a feeding event (Figure 8a, detritus example from 200 m). These particles had equivalent diameters on the order of 70 μm across both sampling events. These particle layers did not appear to be coincident with any pycnoclines or subsurface chlorophyll maxima within the water column (Figures 8, S16 and S17). The location of the layer generally corresponds to the bottom of the WW (Figures S16a, S16c, S16e and S16g in Supporting Information S1).

4. Discussion

4.1. The Subsurface Recirculating Eddy

Mean current velocities from the surface to 300 m in ROMS illustrate cyclonic circulation over PDC during the austral summer (Figure 2). The cyclonic currents are on the order of 10 cm s^{-1} and rotate around a low-pressure system evident in the mean SSH anomaly from the model simulations (Figure 2). This rotation was not perfectly aligned with the canyon in the surface eddy but is stretched southward (Figures 2 and 5). As water moves into the canyon, it moves along isobaths, driven by both bathymetric steering and the low-pressure system observed in the SSH (Figure 2). These observations suggest that the flow in the model is barotropic. Daily average currents suggest that this feature is most coherent in the austral summer and the flow is possibly dominated by other forces the rest of the year (Movie S1). This cyclonic circulation in the model was also observed at the surface by HFR in long (> 12 h) periods of low winds which coincided with periods of weak stratification over the canyon (Figures 5 and S7 in Supporting Information S1) suggesting that at times of low stratification and low wind, the subsurface eddy influences the surface flow.

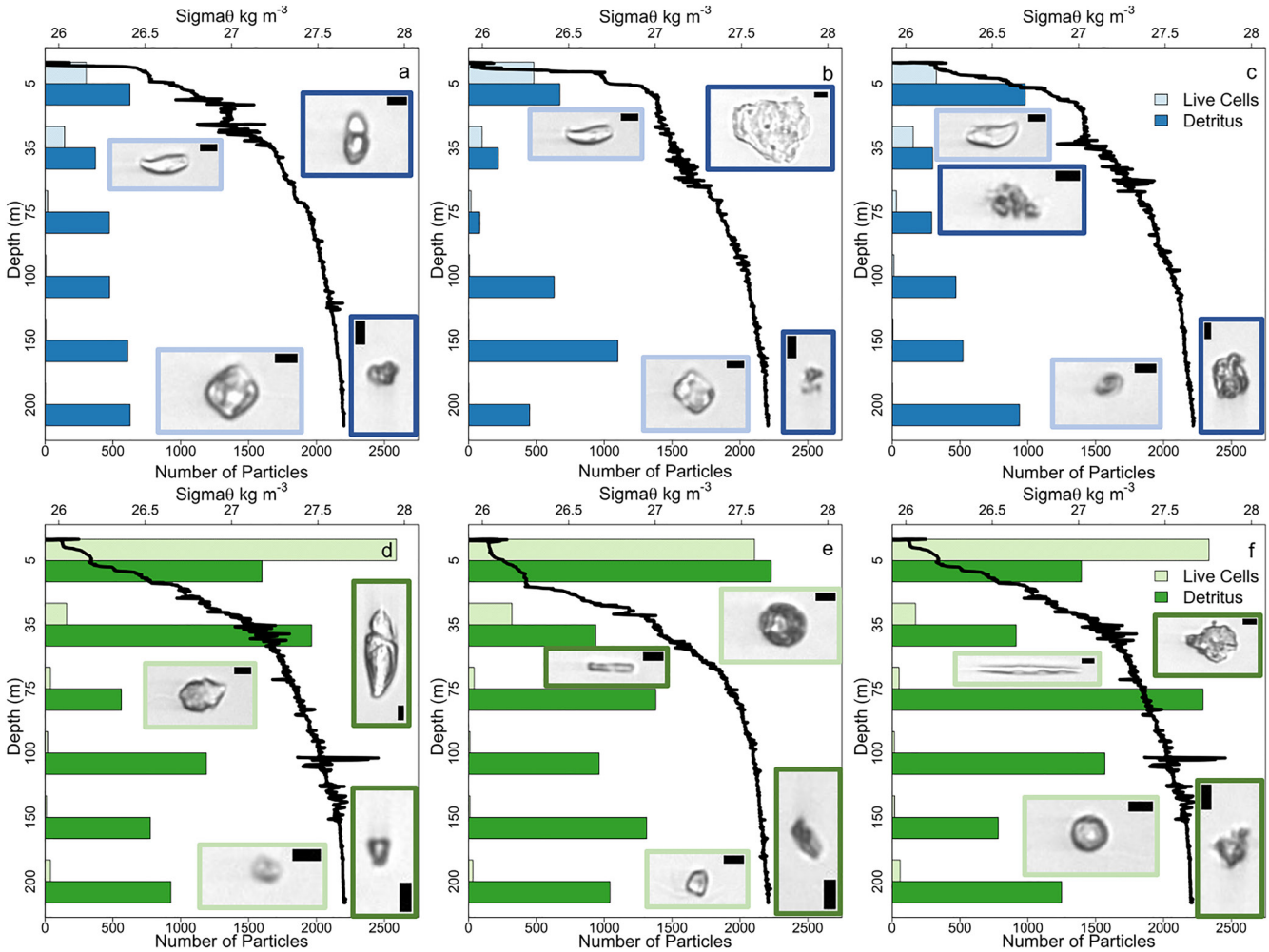

Figure 8. Number of particles (bars) for both live (light colors) and detritus (dark colors) particles counted by the IFCB at three stations: H1 (a–d), H3 (b–e), and H5 (c–f). The top row (a–c) illustrates data from the first IFCB sampling event on February 8, 2020 and the bottom row (d-f) represents data from the second sampling event on March 7, 2020. The black line on each panel represents σ_θ calculated from CTD casts during the sampling event. Photo insets depict examples of live (light border) and detritus (dark border) cells from 5 m (top) and 200 m (bottom) samples. Images represent particles of the approximate median equivalent diameter from each sample. A 5 μm scale bar is provided in each inset.

Averaged cross sections from ROMS (Figure 3) and glider deployments (Figure 4) illustrate doming of isopycnals over PDC. These are most evident in the along-canyon and shelf-canyon lines (Figures 3a and 3b and 4a–4c) and are visible in temperature space (Figures S2a, S2b and S5a–S5c in Supporting Information S1). On the along-canyon and shelf-canyon lines in model simulations and glider observations, isopycnals become shallower above 200 m as the canyon deepens (Figures 3b and 4c). While the locations and depths of the isopycnals between ROMS and glider observations are not identical, the patterns of isopycnal doming above 200 m are similar. This doming of isopycnals over the canyon suggests that there is a baroclinic component to the flow. Isopycnals also appeared to stretch as waters moved over the canyon, and currents follow contours of vorticity, suggesting that conservation of vorticity could play a role in the rotation (Figure S18 in Supporting Information S1). How much of the flow is driven by baroclinic versus barotropic components, and the role of conservation of vorticity, should be investigated further.

The persistence of the eddy in the surface as predicted by the model was not observed in the HFR (Figures 2a and 5). The eddy was only present in the HFR field once each year, while the model suggested it was a semi-persistent feature in the surface (Figure 2a). Therefore, despite the eddy having a clear surface signal in ROMS simulations, we believe the eddy is a primarily subsurface feature. Note that there was a surface signature of the eddy in the HFR observations when the winds and stratification are weak, and

the model is generally less stratified over PDC than observations (Section 3.1.2, Figures 4a–4b, S2, S3, S5a, S5b, S6a and S6b in Supporting Information S1). These differences may be due to factors that impact stratification and water column structure in the summer including missing sources of coastal freshwater, e.g. coastal runoff and iceberg melting (Regan et al., 2018), variations in sea ice cover during the previous winter (Venables et al., 2013), amount and timing of ice melt (Venables et al., 2013; Vernet et al., 2008), and wind mixing (Schofield et al., 2018). The summer MLD over the canyon is deeper in the model than the glider observations (Figure S12 in Supporting Information S1), which may indicate a missing near coast buoyancy source. In addition, the WW layer is less resolved in ROMS while this water mass is a prevalent feature in glider observations. Together, these differences likely led to the model circulation being more barotropic than observations, while the observed circulation shows less indication of the semi-permanent eddy than the model. We believe that these data support our hypothesis that a subsurface recirculating eddy is present within PDC during the austral summer.

4.2. The Retentive Properties of the Eddy

Simulated neutrally buoyant particle experiments illustrate that residence times within PDC increase with depth (Figure 6). We hypothesize that residence times below the surface mixed layer increase significantly as flow becomes more closely aligned with isobaths, forming a closed eddy (Figure 2). The residence times in PDC are much longer than the peak biological season (~60 days), from mid-December to mid/late February. These residence time calculations suggest that retention is high within PDC as a result of the eddy during the austral summer and that particles could be retained for the entire season. The gliders deployed in 2020 also observed low oxygen saturations at depth within the canyon, indicating that this water has not been in contact with the atmosphere for some time, which has been used as a proxy for residence times (Figure S10 in Supporting Information S1; Levin, 2003; Sarmiento et al., 1988). This supports our hypothesis that the subsurface eddy is retentive.

Calculated residence times vary significantly between the surface and at depth (Figure 6). This suggests that PDC is a two-layer system–a surface mixed layer with lower residence times and a deep layer with significantly higher residence times. A significant difference between the surface and 50 m residence times may suggest that 50 m is the approximate bottom of this surface layer in model simulations. Previous observations within PDC also indicate that this two-layer water column structure is present (Hudson et al., 2019). Spatial correlations suggested that surface waters in PDC are not influenced by the canyon, while middepth waters (~100 m) are strongly influenced by the canyon (Hudson et al., 2019). Short residence times in the surface versus increased residence times at depth is similar to the patterns in the previously published spatial correlations, providing further evidence that the PDC strongly influences subsurface flow but not near surface flows.

Residence times appear to vary seasonally, and these variations are amplified at depth. In early December, residence times at 120 m were approximately 15 days (Figure S11 in Supporting Information S1). In mid-December, residence times spiked to approximately 200 days (Figure S11 in Supporting Information S1). There was another spike in residence times at 50 m in late December, reaching a maximum of approximately 40 days (Figure S11 in Supporting Information S1). These spikes are coincident with shoaling of the mixed layer and seasonal variations in model MLD (Figure S12 in Supporting Information S1). As the stratification strengthens at the beginning of the summer, waters deeper than ~150 m are less impacted by surface forcing, and more of the flow is driven by the canyon bathymetry, thus trapping particles in the canyon. At deeper depths (300 m), residence times were consistent with no changes corresponding with seasonal changes in stratification, suggesting that the increasing stratification increases residence times down to a specific depth, having no impact on residence times at depths deeper than this threshold.

While residence times in the surface are similar to previous studies based on HFR observations (4.1 ± 3.3 days in this study vs. 2.1 ± 0.9 days in Kohut et al., 2018), residence times calculated at 150 m are over 100 days greater than previously calculated subsurface residence times for particles released at similar depths (166.6 ± 74 vs. ~50 days; Couto et al., 2017). Previous calculations were made with an older version of the circulation model with 4 km horizontal resolution, over a single month for several model years, coarser and less accurate bathymetry for the region around PDC, and no tidal forcing. It is unclear whether the increased time period, model resolution, or the addition of tides are the cause of these differences.

Preliminary comparisons of residence times in model runs with and without tides within the same season suggest that the addition of tides significantly increases residence times via tidal rectification (Loder, 1980), but this needs to be examined further.

4.3. The Subsurface Particle Layer

Over the deepest portions of the canyon, the particle layer persisted between approximately 75 and 200 m, in 2015 and 2020 (Figures 7a, 7b and 7d). There were almost no particles observed on the continental shelf outside of the canyon, and particle concentrations were significantly lower on the continental shelf outside PDC (Figure 7c). This provides further support for our hypothesis that the subsurface eddy generated by the canyon plays a role in retaining these particles.

Most of the particles in the water column and in the particle layer were detritus. This supports our hypothesis that particles could be marine snow. However, the median equivalent diameter of the particles was smaller than expected for marine snow, which is on the order of 500 μm (Alldredge & Silver, 1988). Instead of aggregates of marine snow, most particles in the particle layer were individual pieces ≤100 μm.

Some cells within the particle layer did consist of small aggregations of individual cells, but most appeared to be individual cells or cell fragments. Many particles looked like they had been sloughed off individuals in a molting event. They could have also been remnants of incomplete or "sloppy" zooplankton feeding (Møller et al., 2003; Roy et al., 1989). It is also possible that these particles may have been remnants of larger, rapidly sinking particles from the surface layer (Bacon et al., 1985; Lal, 1980). While there were identifiable diatoms and other phytoplankton cells in the surface, it was not possible to identify many of the particles in the subsurface layer. Large aggregates of marine snow could have been broken up *in-situ* by small zooplankton, during sampling, or by the IFCB. These particles are organic, and likely sourced from the surface layer. A lower concentration of particles in 2020 in comparison to 2015 and corresponding patterns in surface biomass suggest the surface is a possible source for this particle layer. This would support the theory that suspended particle layers are remnants of larger, rapidly sinking surface particles (Bacon et al., 1985; Lal, 1980).

4.4. Possible Implications for the Biological Hotspot

We have described a persistent subsurface eddy that is present within PDC over the austral summer. This feature is formed by water moving along isobaths as it moves into the canyon and potentially plays a role ecologically by retaining particles over PDC. Given that the eddy is only present in the surface when winds are low and stratification is weak for long periods of time, we believe that this feature occurs primarily below the mixed layer. Therefore, we believe the eddy has the largest effects on consumers, rather than primary producers.

In addition, this study and previous work have shown that the surface mixed layer and subsurface waters are decoupled, with subsurface waters impacted by the presence of the canyon while surface waters are nearly unaffected by its presence (Hudson et al., 2019). Therefore, we would not expect this subsurface eddy to have an effect on the sea surface temperature, sea ice concentration, and chlorophyll patterns observed over PDC as posited by Kavanaugh et al. (2015). Possible explanations for the driving factors behind these satellite-based observations, beyond local upwelling of mUCDW, include local katabatic winds or strong surface currents, leading to the low-ice conditions observed by Kavanaugh et al. (2015) (Hudson et al., 2019). Recent experiments with local phytoplankton populations have suggested that phytoplankton within PDC are light, rather than nutrient limited (Carvalho et al., 2020). If the system is light limited, low-ice conditions, like those seen in PDC, and other similar coastal canyon systems along the WAP, would increase surface irradiance, hence driving the increased sea surface temperature and chlorophyll concentrations observed by Kavanaugh et al. (2015) (Hudson et al., 2019; Schofield et al., 2013; Smith & Gordon, 1997).

The particle layer retained within the canyon could play a role in the maintenance of a biological hotspot in terms of enhanced microbial activity and zooplankton grazing. Sloppy feeding by zooplankton has been shown to act as a significant source of dissolved organic carbon to the microbial food web (Møller et al., 2003). In addition, subsurface organic particle layers worldwide have been associated with increased

microbial activity (Alldredge & Silver, 1988; Garfield et al., 1983). Suspended subsurface particle layers may play a large role in sustaining mesopelagic heterotrophs (Baltar et al., 2009, 2010; Duret et al., 2019). Recent work suggests that distinct microbial communities form on suspended rather than sinking detritus particles in mesopelagic and mixed layers of the Scotia Sea, north of the WAP (Duret et al., 2019). These communities are uniquely adapted to utilize differing amounts of organic carbon and play different roles in the biological carbon pump (Duret et al., 2019). The suspended particle layer in PDC may be similar and could play a critical role in the local biological pump and remineralization of nutrients.

The subsurface particle layer may also act as an important food source for local zooplankton. Isotope analysis around Hawaii has shown that micronekton are more reliant on suspended particles for food as habitat depth increases (Gloeckler et al., 2018). The same study reported that several fish species feed primarily on suspended particles. Several detritivorous zooplankton species can be found at mesopelagic depths along the WAP (Conroy et al., 2020). These zooplankton species could potentially feed on the subsurface particle layer, which ranged between 75 and 200 m. Residence times at these depths ranged from 18 $\pm$ 10.2 to 167 $\pm$ 74 days (Figure 6), so this food source could persist through the austral summer at greater depths.

Antarctic krill have been observed feeding on detritus (for example, Kawaguchi et al., 1986; Quetin & Ross, 1991; Schmidt et al., 2012, 2014; and others). Therefore, they could potentially utilize the subsurface particle layer as a food source. However, it is unclear if and how often krill utilize detritus as a food source during the austral summer. Most observations of krill feeding on detritus have occurred during the winter when food concentrations are low (Schmidt & Atkinson, 2016). If they feed on detritus in the austral summer in similar conditions, it may be a key food source when chlorophyll concentrations are low.

It is unclear if the subsurface particle layer, and the eddy responsible for retaining it over PDC, persists into winter. Daily mean currents at 100 m from ROMS suggest that the eddy is most persistent over PDC from mid-to-late December into early March (Movie S1). Wintertime ROMS particle simulations of the subsurface particle layer are necessary to understand if this subsurface particle layer can act as a food source for zooplankton in these food-limited months.

It is also possible that the subsurface eddy retains zooplankton. Most zooplankton, including calanoid copepods, live at predominantly low Reynolds numbers (Koehl & Strickier, 1981; Price, 1988) and could be trapped within this recirculating eddy, since they would not be able to swim against the prevailing currents. Zooplankton retention within eddies has been observed in the subarctic North Pacific (Mackas et al., 2005) and in the Irish Sea (Emsley et al., 2005). Zooplankton, including the Antarctic krill, are a critical food source for local predator species (Fraser & Hofmann, 2003; Pickett et al., 2018). Depending on their size, zooplankton may live at the low Reynolds numbers required to facilitate retention in the subsurface eddy. Many zooplankton perform diel vertical migrations, spending their days at depth, and feeding in the surface at night when visual predation risk is low (Hays, 2008). The vertical migration behavior may interact with the two-layer hydrography present within PDC as suggested by this study and previous glider observations (Hudson et al., 2019). Zooplankton may be retained at depth within the eddy during the day. At night, horizontal advection in the surface layer could transport zooplankton elsewhere. Previous HFR deployments suggested that surface currents over the canyon moves predominately toward shore (Bernard et al., 2017; Kohut et al., 2018). Zooplankton could possibly be advected into these nearshore regions during their time in the surface layer, where predator foraging activity is highest. Therefore, the eddy may serve as a major retainer and delivery mechanism of important resources near these higher trophic level foraging grounds. The relationship of these higher trophic levels with this subsurface eddy, should be explored further to determine if the eddy is responsible for the presence of this biological hotspot.

Data Availability Statement

Glider data used in this analysis can be accessed at the glider ERDDAP server (https://gliders.ioos.us/erddap/info/index.html). HFR data from 2015 and 2020 are also available on ERDDAP (http://hfr.marine.rutgers.edu/erddap/griddap/converge_reprocess.graph and https://hfr.marine.rutgers.edu/erddap/griddap/swarm_25mz_totals_reprocessed_with_qc_radials.html). Wind data from 2015 are available at NCEI (https://www.ncei.noaa.gov/access/metadata/landing-page/bin/iso?id=gov.noaa.nodc:0187193). ROMS particle simulations; ROMS temperature, salinity, and density data; Imaging Flow Cytobot feature data

and associated CTD data; and wind data from 2020 are available on BCO-DMO (https://www.bco-dmo.org/project/850844).

Acknowledgments
This project was funded through the National Science Foundation, Award Numbers 1327248 (2015) and 1744884 (2020) to UD, 1744884 to RU, and 1745011 to ODU. We are grateful to the Antarctic Support Contractor and their teams in Denver, CO, aboard the RVIB Laurence M. Gould, and at Palmer Station, without whom a project such as this would not be possible. We thank the students and field assistants from both projects for their valuable work on this project and the Palmer Antarctica Long-Term Ecological Research team for their involvement, suggestions, and collaboration. Computer simulations were run on the Wahab High Performance computing cluster at ODU.

References

Alldredge, A. L., & Silver, M. W. (1988). Characteristics, dynamics and significance of marine snow. *Progress in Oceanography*, *20*(1), 41–82. https://doi.org/10.1016/0079-6611(88)90053-5

Bacon, M. P., Huh, C.-A., Fleer, A. P., & Deuser, W. G. (1985). Seasonality in the flux of natural radionuclides and plutonium in the deep Sargasso Sea. *Deep-Sea Research Part A. Oceanographic Research Papers*, *32*(3), 273–286. https://doi.org/10.1016/0198-0149(85)90079-2

Baltar, F., Arístegui, J., Gasol, J. M., Sintes, E., & Herndl, G. J. (2009). Evidence of prokaryotic metabolism on suspended particulate organic matter in the dark waters of the subtropical North Atlantic. *Limnology and Oceanography*, *54*(1), 182–193. https://doi.org/10.4319/lo.2009.54.1.0182

Baltar, F., Arístegui, J., Sintes, E., Gasol, J. M., Reinthaler, T., & Herndl, G. J. (2010). Significance of non-sinking particulate organic carbon and dark CO_2 fixation to heterotrophic carbon demand in the mesopelagic northeast Atlantic. *Geophysical Research Letters*, *37*(9). https://doi.org/10.1029/2010GL043105

Barrick, D. E., Lipa, B. J., & Crissman, R. D. (1985). Mapping surface currents with CODAR. *Sea Technology*, *26*(10), 43–48.

Bernard, K. S., Cimino, M., Fraser, W., Kohut, J., Oliver, M. J., Patterson-Fraser, D., et al. (2017). Factors that affect the nearshore aggregations of Antarctic krill in a biological hotspot. *Deep Sea Research Part I: Oceanographic Research Papers*, *126*, 139–147. https://doi.org/10.1016/j.dsr.2017.05.008

Budgell, W. P. (2005). Numerical simulation of ice-ocean variability in the Barents Sea region: Towards dynamical downscaling. *Ocean Dynamics*, *55*(3–4), 370–387. https://doi.org/10.1007/s10236-005-0008-3

Carvalho, F., Fitzsimmons, J. N., Couto, N., Waite, N., Gorbunov, M., Kohut, J., et al. (2020). Testing the Canyon Hypothesis: Evaluating light and nutrient controls of phytoplankton growth in penguin foraging hotspots along the West Antarctic Peninsula. *Limnology and Oceanography*, *65*(3), 455–470. https://doi.org/10.1002/lno.11313

Carvalho, F., Kohut, J., Oliver, M. J., & Schofield, O. (2017). Defining the ecologically relevant mixed-layer depth for Antarctica's coastal seas: MLD in Coastal Antarctica. *Geophysical Research Letters*, *44*(1), 338–345. https://doi.org/10.1002/2016GL071205

Carvalho, F., Kohut, J., Oliver, M. J., Sherrell, R. M., & Schofield, O. (2016). Mixing and phytoplankton dynamics in a submarine canyon in the West Antarctic Peninsula: Phytoplankton dynamics in Wap canyon. *Journal of Geophysical Research: Oceans*, *121*(7), 5069–5083. https://doi.org/10.1002/2016JC011650

Conroy, J. A., Steinberg, D. K., Thibodeau, P. S., & Schofield, O. (2020). Zooplankton diel vertical migration during Antarctic summer. *Deep Sea Research Part I: Oceanographic Research Papers*, *162*, 103324. https://doi.org/10.1016/j.dsr.2020.103324

Couto, N., Kohut, J., Schofield, O., Dinniman, M., & Graham, J. (2017). Pathways and retention times in a biologically productive canyon system on the West Antarctic Peninsula. *OCEANS 2017 - Anchorage*, *1–8*.

Dinniman, M. S., Klinck, J. M., & Hofmann, E. E. (2012). Sensitivity of circumpolar deep water transport and Ice Shelf basal melt along the West Antarctic Peninsula to changes in the winds. *Journal of Climate*, *25*(14), 4799–4816. https://doi.org/10.1175/JCLI-D-11-00307.1

Dinniman, M. S., Klinck, J. M., & Smith, W. O. (2011). A model study of circumpolar deep water on the West Antarctic Peninsula and Ross Sea continental shelves. *Deep Sea Research Part II: Topical Studies in Oceanography*, *58*(13–16), 1508–1523. https://doi.org/10.1016/j.dsr2.2010.11.013

Duret, M. T., Lampitt, R. S., & Lam, P. (2019). Prokaryotic niche partitioning between suspended and sinking marine particles. *Environmental Microbiology Reports*, *11*(3), 386–400. https://doi.org/10.1111/1758-2229.12692

Emsley, S. M., Tarling, G. A., & Burrows, M. T. (2005). The effect of vertical migration strategy on retention and dispersion in the Irish Sea during spring–summer. *Fisheries Oceanography*, *14*(3), 161–174. https://doi.org/10.1111/j.1365-2419.2005.00327.x

Emslie, S., Fraser, W., Smith, R., & Walker, W. (1998). Abandoned penguin colonies and environmental change in the Palmer Station area, Anvers Island, Antarctic Peninsula. *Antarctic Science*, *10*, 257–268. https://doi.org/10.1017/S0954102098000352

Emslie, S. D., & Patterson, W. P. (2007). Abrupt recent shift in 13C and 15N values in Adelie penguin eggshell in Antarctica. *Proceedings of the National Academy of Sciences*, *104*(28), 11666–11669. https://doi.org/10.1073/pnas.0608477104

Fraser, W., & Hofmann, E. (2003). A predator's perspective on causal links between climate change, physical forcing and ecosystem response. *Marine Ecology Progress Series*, *265*, 1–15. https://doi.org/10.3354/meps265001

Fraser, W. R., & Trivelpiece, W. Z. (1996). Factors controlling the distribution of seabirds: Winter-summer heterogeneity in the distribution of adélie penguin populations. In E. E. Hofmann, R. M. Ross, & L. B. Quetin (Eds.), *Antarctic research series* (Vol. *70*, pp. 257–272). American Geophysical Union. https://doi.org/10.1029/AR070p0257

Fretwell, P., Pritchard, H. D., Vaughan, D. G., Bamber, J. L., Barrand, N. E., Bell, R., et al. (2013). Bedmap2: Improved ice bed, surface and thickness datasets for Antarctica. *The Cryosphere*, *7*(1), 375–393. https://doi.org/10.5194/tc-7-375-2013

Garfield, P. C., Packard, T. T., Friederich, G. E., & Codispoti, L. A. (1983). A subsurface particle maximum layer and enhanced microbial activity in the secondary nitrite maximum of the northeastern tropical Pacific Ocean. *Journal of Marine Research*, *41*(4), 747–768. https://doi.org/10.1357/002224083788520496

Gloeckler, K., Choy, C. A., Hannides, C. C. S., Close, H. G., Goetze, E., Popp, B. N., & Drazen, J. C. (2018). Stable isotope analysis of micronekton around Hawaii reveals suspended particles are an important nutritional source in the lower mesopelagic and upper bathypelagic zones. *Limnology and Oceanography*, *63*(3), 1168–1180. https://doi.org/10.1002/lno.10762

Graham, J. A., Dinniman, M. S., & Klinck, J. M. (2016). Impact of model resolution for on-shelf heat transport along the West Antarctic Peninsula. *Journal of Geophysical Research: Oceans*, *121*(10), 7880–7897. https://doi.org/10.1002/2016JC011875

Haidvogel, D. B., Arango, H., Budgell, W. P., Cornuelle, B. D., Curchitser, E., Di Lorenzo, E., et al. (2008). Ocean forecasting in terrain-following coordinates: Formulation and skill assessment of the Regional Ocean Modeling System. *Journal of Computational Physics*, *227*(7), 3595–3624. https://doi.org/10.1016/j.jcp.2007.06.016

Hays, G. C. (2008). A review of the adaptive significance and ecosystem consequences of zooplankton diel vertical migrations. *Hydrobiologica*, *503*, 163–170.

Holland, D. M., & Jenkins, A. (1999). Modeling thermodynamic ice–ocean interactions at the base of an ice shelf. *Journal of Physical Oceanography*, *29*, 15. https://doi.org/10.1175/1520-0485(1999)029<1787:mtioia>2.0.co;2

Hudson, K., Oliver, M. J., Bernard, K., Cimino, M. A., Fraser, W., Kohut, J., et al. (2019). Reevaluating the canyon hypothesis in a biological hotspot in the western Antarctic Peninsula. *Journal of Geophysical Research: Oceans*, *124*(8), 6345–6359. https://doi.org/10.1029/2019JC015195

Hunter, J. R., Craig, P. D., & Phillips, H. E. (1993). On the use of random walk models with spatially variable diffusivity. *Journal of Computational Physics*, *106*(2), 366–376. https://doi.org/10.1016/S0021-9991(83)71114-9

Kavanaugh, M., Abdala, F., Ducklow, H., Glover, D., Fraser, W., Martinson, D., et al. (2015). Effect of continental shelf canyons on phytoplankton biomass and community composition along the western Antarctic Peninsula. *Marine Ecology Progress Series*, *524*, 11–26. https://doi.org/10.3354/meps11189

Kawaguchi, K., Matsuda, O., Ishikawa, S., & Naito, Y. (1986). A light trap to collect krill and other micronektonic and planktonic animals under the Antarctic coastal fast ice. *Polar Biology*, *6*(1), 37–42. https://doi.org/10.1007/BF00446238

Kelley, D., & Richards, C. (2020). *oce: Analysis of oceanographic data (version R package*. Retrieved from https://CRAN.R-project.org/package=oce

Koehl, M. A. R., & Strickier, J. R. (1981). Copepod feeding currents: Food capture at low Reynolds number1. *Limnology and Oceanography*, *26*(6), 1062–1073. https://doi.org/10.4319/lo.1981.26.6.1062

Kohut, J. T., Winsor, P., Statscewich, H., Oliver, M. J., Fredj, E., Couto, N., et al. (2018). Variability in summer surface residence time within a West Antarctic Peninsula biological hotspot. *Philosophical Transactions of the Royal Society A: Mathematical, Physical and Engineering Sciences*, *376*(2122), 20170165. https://doi.org/10.1098/rsta.2017.0165

Lal, D. (1980). Comments on some aspects of particulate transport in the oceans. *Earth and Planetary Science Letters*, *49*(2), 520–527. https://doi.org/10.1016/0012-821X(80)90093-X

Levin, L. A. (2003). Oxygen minimum zone benthos: Adaptation and community response to hypoxia. *Oceanography and Marine Biology: An Annual Review*, *41*, 1–45.

Loder, J. (1980). Topographic rectification of tidal currents on the sides of georges Bank. *Journal of Physical Oceanography*, *10*, 92. https://doi.org/10.1175/1520-0485(1980)010<1399:trotco>2.0.co;2

Mackas, D. L., Tsurumi, M., Galbraith, M. D., & Yelland, D. R. (2005). Zooplankton distribution and dynamics in a North Pacific Eddy of coastal origin: II. Mechanisms of eddy colonization by and retention of offshore species. *Deep Sea Research Part II: Topical Studies in Oceanography*, *52*(7), 1011–1035. https://doi.org/10.1016/j.dsr2.2005.02.008

Martinson, D. G., & McKee, D. C. (2012). Transport of warm Upper Circumpolar Deep Water onto the western Antarctic Peninsula continental shelf. *Ocean Science*, *8*(4), 433–442. https://doi.org/10.5194/os-8-433-2012

Moffat, C., Owens, B., & Beardsley, R. C. (2009). On the characteristics of Circumpolar Deep Water intrusions to the west Antarctic Peninsula Continental Shelf. *Journal of Geophysical Research*, *114*(C5). https://doi.org/10.1029/2008JC004955

Moline, M. A. (1998). *Temporal dynamics and regulation of coastal Antarctic phytoplankton communities: Spring/summer 1991-1994 (Doctoral dissertation)*. University of California.

Møller, E., Thor, P., & Nielsen, T. (2003). Production of DOC by Calanus finmarchicus, C. glacialis and C. hyperboreus through sloppy feeding and leakage from fecal pellets. *Marine Ecology Progress Series*, *262*, 185–191. https://doi.org/10.3354/meps262185

Oliver, M. J., Irwin, A., Moline, M. A., Fraser, W., Patterson, D., Schofield, O., & Kohut, J. (2013). Adélie Penguin Foraging Location Predicted by Tidal Regime Switching. *PLoS One*, *8*(1), e55163. https://doi.org/10.1371/journal.pone.0055163

Oliver, M. J., Kohut, J. T., Bernard, K., Fraser, W., Winsor, P., Statscewich, H., et al. (2019). Central place foragers select ocean surface convergent features despite differing foraging strategies. *Scientific Reports*, *9*(1). https://doi.org/10.1038/s41598-018-35901-7

Olson, R. J., & Sosik, H. M. (2007). A submersible imaging-in-flow instrument to analyze nano-and microplankton: Imaging FlowCytobot. *Limnology and Oceanography: Methods*, *5*(6), 195–203. https://doi.org/10.4319/lom.2007.5.195

Padman, L., Fricker, H. A., Coleman, R., Howard, S., & Erofeeva, L. (2002). A new tide model for the Antarctic ice shelves and seas. *Annals of Glaciology*, *34*, 247–254. https://doi.org/10.3189/172756402781817752

Pickett, E. P., Fraser, W. R., Patterson-Fraser, D. L., Cimino, M. A., Torres, L. G., & Friedlaender, A. S. (2018). Spatial niche partitioning may promote coexistence of *Pygoscelis* penguins as climate-induced sympatry occurs. *Ecology and Evolution*, *8*(19), 9764–9778. https://doi.org/10.1002/ece3.4445

Piñones, A., Hofmann, E. E., Dinniman, M. S., & Klinck, J. M. (2011). Lagrangian simulation of transport pathways and residence times along the western Antarctic Peninsula. *Deep Sea Research Part II: Topical Studies in Oceanography*, *58*(13), 1524–1539. https://doi.org/10.1016/j.dsr2.2010.07.001

Powers, J. G., Manning, K. W., Bromwich, D. H., Cassano, J. J., & Cayette, A. M. (2012). A DECADE OF ANTARCTIC SCIENCE SUPPORT THROUGH AMPS. *Bulletin of the American Meteorological Society*, *93*(11), 1699–1712. https://doi.org/10.1175/bams-d-11-00186.1

Prézelin, B. B., Hofmann, E. E., Mengelt, C., & Klinck, J. M. (2000). The linkage between Upper Circumpolar Deep Water (UCDW) and phytoplankton assemblages on the west Antarctic Peninsula continental shelf. *Journal of Marine Research*, *58*(2), 165–202. https://doi.org/10.1357/002224000321511133

Prézelin, B. B., Hofmann, E. E., Moline, M., & Klinck, J. M. (2004). Physical forcing of phytoplankton community structure and primary production in continental shelf waters of the Western Antarctic Peninsula. *Journal of Marine Research*, *62*(3), 419–460. https://doi.org/10.1357/0022240041446173

Price, H. J. (1988). Feeding mechanisms in marine and freshwater Zooplankton. *Bulletin of Marine Science*, *43*(3), 17.

Quetin, L. B., & Ross, R. M. (1991). Behavioral and Physiological Characteristics of the Antarctic Krill, *Euphausia superba*. *American Zoologist*, *31*(1), 49–63. https://doi.org/10.1093/icb/31.1.49

R Core Team. (2020). *R: A language and environment for statistical computing*. R Foundation for Statistical Computing. Retrieved from www.R-project.org

Regan, H. C., Holland, P. R., Meredith, M. P., & Pike, J. (2018). Sources, variability and fate of freshwater in the Bellingshausen Sea, Antarctica. *Deep Sea Research Part I: Oceanographic Research Papers*, *133*, 59–71. https://doi.org/10.1016/j.dsr.2018.01.005

Roy, S., Harris, R. P., & Poulet, S. A. (1989). Inefficient feeding by Calanus helgolandicus and Temora longicornis on Coscinodiscus wailesii: Quantitative estimation using chlorophyll-type pigments and effects on dissolved free amino acids. *Marine Ecology Progress Series*, *52*(2), 145–153. https://doi.org/10.3354/meps052145

Ryan, W. B. F., Carbotte, S. M., Coplan, J. O., O'Hara, S., Melkonian, A., Arko, R., et al. (2009). Global multi-resolution topography synthesis: Global multi-resolution topography synthesis. *Geochemistry, Geophysics, Geosystems*, *10*(3). https://doi.org/10.1029/2008GC002332

Sarmiento, J. L., Herbert, T. D., & Toggweiler, J. R. (1988). Causes of anoxia in the world ocean. *Global Biogeochemical Cycles*, *2*(2), 115–128. https://doi.org/10.1029/GB002i002p00115

Schmidt, K., & Atkinson, A. (2016). Feeding and food processing in Antarctic Krill (Euphausia superba Dana). In V. Siegel (Ed.), *Biology and ecology of Antarctic krill* (pp. 175–224). Springer International Publishing. https://doi.org/10.1007/978-3-319-29279-3_5

Schmidt, K., Atkinson, A., Pond, D. W., & Ireland, L. C. (2014). Feeding and overwintering of Antarctic krill across its major habitats: The role of sea ice cover, water depth, and phytoplankton abundance. *Limnology and Oceanography*, *59*(1), 17–36. https://doi.org/10.4319/lo.2014.59.1.0017

Schmidt, K., Atkinson, A., Venables, H. J., & Pond, D. W. (2012). Early spawning of Antarctic krill in the Scotia Sea is fuelled by "superfluous" feeding on non-ice associated phytoplankton blooms. *Deep Sea Research Part II: Topical Studies in Oceanography*, *59–60*, 159–172. https://doi.org/10.1016/j.dsr2.2011.05.002

Schofield, O., Brown, M., Kohut, J., Nardelli, S., Saba, G., Waite, N., & Ducklow, H. (2018). Changes in the upper ocean mixed layer and phytoplankton productivity along the West Antarctic Peninsula. *Philosophical Transactions of the Royal Society A: Mathematical, Physical and Engineering Sciences*, *376*(2122), 20170173. https://doi.org/10.1098/rsta.2017.0173

Schofield, O., Ducklow, H., Bernard, K., Doney, S., Patterson-Fraser, D., Gorman, K., et al. (2013). Penguin biogeography along the West Antarctic Peninsula: Testing the Canyon hypothesis with palmer LTER observations. *Oceanography*, *26*(3), 204–206. https://doi.org/10.5670/oceanog.2013.63

Sherrell, R. M., Annett, A. L., Fitzsimmons, J. N., Roccanova, V. J., & Meredith, M. P. (2018). A 'shallow bathtub ring' of local sedimentary iron input maintains the Palmer Deep biological hotspot on the West Antarctic Peninsula shelf. *Philosophical Transactions of the Royal Society A: Mathematical, Physical and Engineering Sciences*, *376*(2122), 20170171. https://doi.org/10.1098/rsta.2017.0171

Smith, R. C., Baker, K. S., Fraser, W. R., Hofmann, E. E., Karl, D. M., Klinck, J. M., et al. (1995). The Palmer LTER: A long-term ecological research program at palmer station, Antarctica. *Oceanography*, *8*(3), 77–86. https://doi.org/10.5670/oceanog.1995.01

Smith, W. O., & Gordon, L. I. (1997). Hyperproductivity of the Ross Sea (Antarctica) polynya during austral spring. *Geophysical Research Letters*, *24*(3), 233–236. https://doi.org/10.1029/96GL03926

Venables, H. J., Clarke, A., & Meredith, M. P. (2013). Wintertime controls on summer stratification and productivity at the western Antarctic Peninsula. *Limnology and Oceanography*, *58*(3), 1035–1047. https://doi.org/10.4319/lo.2013.58.3.1035

Vernet, M., Martinson, D., Iannuzzi, R., Stammerjohn, S., Kozlowski, W., Sines, K., et al. (2008). Primary production within the sea-ice zone west of the Antarctic Peninsula: I—Sea ice, summer mixed layer, and irradiance. *Deep Sea Research Part II: Topical Studies in Oceanography*, *55*(18–19), 2068–2085. https://doi.org/10.1016/j.dsr2.2008.05.021

Visser, A. (1997). Using random walk models to simulate the vertical distribution of particles in a turbulent water column. *Marine Ecology Progress Series*, *158*, 275–281. https://doi.org/10.3354/meps158275